

Prediction of the hot flow behaviour of a third generation advanced high-strength hot-formable steel

Philipp Althaus^{1,*}, Radhakanta Rana², Hendrik Wester¹, Johanna Uhe¹, and Bernd-Arno Behrens¹

¹ Leibniz University Hannover, Institute of Forming Technology and Machines, 30823 Garbsen, Germany

² Tata Steel, Wenckebachstraat 1, 1970 CA IJmuiden, The Netherlands

Received: 4 July 2025 / Accepted: 9 January 2026

Abstract. Medium manganese steels provide numerous benefits in hot forming, including reduced blank reheating temperatures and critical quenching rates compared to conventional boron-added steels. Moreover, their enhanced strength and ductility make them a promising material for lightweight components in the mobility sector. In this study, the flow behaviour of a novel medium manganese steel is characterised and modelled to enable the simulation of hot forming processes. A forming and quenching dilatometer is utilised for isothermal tensile tests at different forming temperatures and strain rates. The specimens undergo heat treatment prior to forming, following a process route that includes annealing, cooling, and reheating to replicate the heat treatment at the steel producer and the hot forming at the parts manufacturer. An in-situ optical measurement system is used to determine the strains with digital image correlation. The experimental flow curves are modelled using various phenomenological hardening laws. Finally, the applicability of the hardening laws is verified by the simulation of a tensile test that was not used for modelling. The best prediction accuracy was achieved by the modified Norton-Hoff law, which provided a root mean square error of 14.4% during model calibration and a low mean absolute percentage error of 1.3% during validation.

Keywords: Medium manganese steel / hot forming / deformation characterisation / flow behaviour

1 Introduction

In the mobility sector, demands concerning passenger safety, CO₂ emissions and fuel consumption are growing. Moreover, additional components for comfort are being incorporated into new vehicles. To meet the requirements of safe, comfortable and environmentally sustainable transportation, lightweight construction remains essential in the mobility industry [1,2]. Hot forming is a well-established method to produce lightweight, high-strength components [2,3]. In hot forming, a sheet metal is reheated in a large roller hearth furnace above the austenite transformation temperature, then transferred to a press where it is formed using water-cooled stamping tools, resulting in rapid quenching. The high quenching rate results in a completely martensitic microstructure after forming, which leads to very high strengths but low ductility. Therefore, hot forming is primarily employed in the automotive sector to manufacture components that are relevant to safety, including A-, B- and C-pillars, bumpers and cross beams [2,4]. For these components, the use of boron-added steels like 22MnB5 grade (also known as

'boron steel') has been established in industry, which are reheated to around 900–950 °C prior to forming in order to achieve full austenitisation [5].

Current research on hot-forming steels focuses on the improvement of the in-service mechanical properties of the steels as well as the optimisation of the efficiency of the hot forming process. In this context, medium manganese steels are increasingly investigated for the potential use in hot forming [6–10]. Medium Mn steels have a manganese content ranging from 3 to 12 wt.% [11–14]. These materials are a type of the third generation of advanced high-strength steels (3G-AHSS) and provide a remarkable balance of strength and ductility, which is largely attributed to the transformation-induced plasticity (TRIP) effect [15]. The microstructure of medium Mn steels typically consists of ferrite, martensite and retained austenite (RA), which is in a metastable condition. During forming, the RA transforms to martensite, leading to high strains and increased work hardening, resulting in delayed necking before fracture. Apart from their excellent mechanical properties, medium Mn steels provide benefits in processing. Unlike traditional boron steels, they can be formed after reheating at lower temperatures [7–9,16] and with lower critical cooling rates [17], facilitating energy savings during production. In addition to their high strength-ductility combination,

* e-mail: althaus@ifum.uni-hannover.de

medium Mn steels exhibit high wear resistance, making them suitable for further applications such as in the mining industry [18].

Although hot forming of established boron steels is considered state-of-the-art and has been studied by many researchers, medium Mn steels are still in their early stage of development. Recent studies analysed the effects of the alloy composition and optimal processing parameters for improved properties during and after forming. Bilir et al. investigated the thermo-mechanical behaviour of a novel medium Mn steel for the simulation of a hot stamping process by means of the finite element (FE) software PAM-STAMP [19]. Due to its greater hardenability, the medium Mn steel was found to be unaffected by variations in transfer or quenching times, unlike the 22MnB5 grade. Consequently, the costs for tool making can be reduced because of lower cooling demands and more complex components with greater sheet thicknesses can be formed. Zheng et al. carried out deep drawing experiments and simulations to compare the formability of a newly developed medium Mn steel to that of 22MnB5 grade [20]. The medium Mn steel showed superior formability due to its more compact and uniform martensitic structure and thickness distribution after hot forming.

Many authors employ the finite element method (FEM) as an effective tool to save time and costs in process design while facilitating a more profound comprehension of underlying mechanisms. However, in order to obtain a high prediction accuracy of the simulation results, a realistic modelling of the material behaviour is crucial. One of the primary input parameters to model the material behaviour during forming is the flow curve. It specifies the evolution of the yield surface and describes the work hardening of the material during forming. In hot forming, the process of plastic deformation occurs at the same time as quenching due to the contact of the hot blank with the colder tools. Thus, it is important to characterise the flow behaviour at various temperatures and strain rates in the range of the forming process [21].

Tong et al. examined the flow behaviour of a medium Mn steel containing 8 wt.% Mn under hot stamping conditions using uniaxial tensile tests [22]. Higher forming temperatures resulted in a significant reduction of the true stress, while higher strain rates caused a moderate increase of the true stress. The total elongation was found to be unaffected by varying forming temperatures and strain rates. Lin et al. examined the high-temperature flow behaviour of a medium-high carbon Mn-Si-Cr steel using hot compression tests [23]. Two constitutive models were used to model the flow stresses taking work hardening, dynamic recovery, and dynamic recrystallisation into account. A strain-compensated Arrhenius-type model and a multiple-linear model accurately predicted the flow stresses across a wide range of conditions. The multiple-linear model showed a slightly higher accuracy and an easier application due to a simpler structure. Yan et al. also applied compression tests to investigate the hot deformation behaviour of a medium Mn steel with ~9 wt.% Mn [24]. The steel exhibited significant flow softening over 950 °C and lower strain rates due to dynamic recrystallisation and flow instability. Constitutive equations were developed to

accurately model the flow behaviour based on the modified-Arrhenius equation taking the effects of strain, strain rate, and temperature into account. Li et al. studied the effect of the heating process on the microstructure and deformation behaviour of a medium Mn steel with 4.76 wt.% Mn during warm deformation between temperatures of 550 °C and 850 °C [25]. It was found that when the microstructure consists solely of austenite, the steel shows excellent work hardening capability, gradually balancing hardening and softening. In contrast, the presence of ferrite during deformation led to poor work-hardening capability leading to a peak stress at low strains, followed by dynamic softening. Xu et al. investigated the hot flow behaviour of conventional hot forming steel grade 22MnB5 by conducting isothermal compression tests between 800 °C and 950 °C and various strain rates [26]. A physical constitutive model incorporating work hardening, dynamic recovery, and dynamic recrystallisation was developed and a good prediction accuracy was demonstrated by a high correlation coefficient and a low average error. It was also found that the martensite morphology after hot forming and quenching is significantly influenced by the deformation conditions, with a lower temperature and higher strain rate resulting in finer martensite packets. Zhou et al. also investigated the thermo-mechanical behaviour of 22MnB5 steel grade at various temperatures and strain rates using isothermal tensile tests [27]. A modified Arrhenius-type constitutive model was effectively applied to describe the flow behaviour with less than 5% relative error.

In this paper, the flow behaviour of a novel medium Mn steel with a relatively low Mn content of 4.5 wt.% is characterised at various temperatures and strain rates and modelled using different phenomenological hardening laws to enable the simulation and design of hot forming processes. An initial modelling approach was carried out previously in reference [28], but in the present paper a more optimised heat treatment route is investigated which leads to better mechanical properties of the medium Mn steel. Furthermore, the tensile tests are carried out in a wider temperature range and an in-situ optical measurement system is used to calculate the strains of the specimen surface with digital image correlation. For a proper validation of the modelled flow curves, an additional tensile test is conducted which is not used for the model calibration.

2 Material and methods

The medium Mn steel sheets investigated in this study were uncoated and in a cold rolled condition with a dimension of 1000 mm × 100 mm and a thickness of 1.5 mm. Using dilatometry with a heating rate of 5 °C/s, the austenite transformation start (A_{c1}) and finish (A_{c3}) temperatures of the steel were determined as 611 °C and 780 °C, respectively. To evaluate flow curves within the hot forming relevant process range, isothermal tensile tests were performed. A quenching and forming dilatometer DIL 805A/D/T from TA Instruments was used for this purpose. Figure 1a shows the dilatometer with the schematic test setup and specimen geometry. In a previous work, the

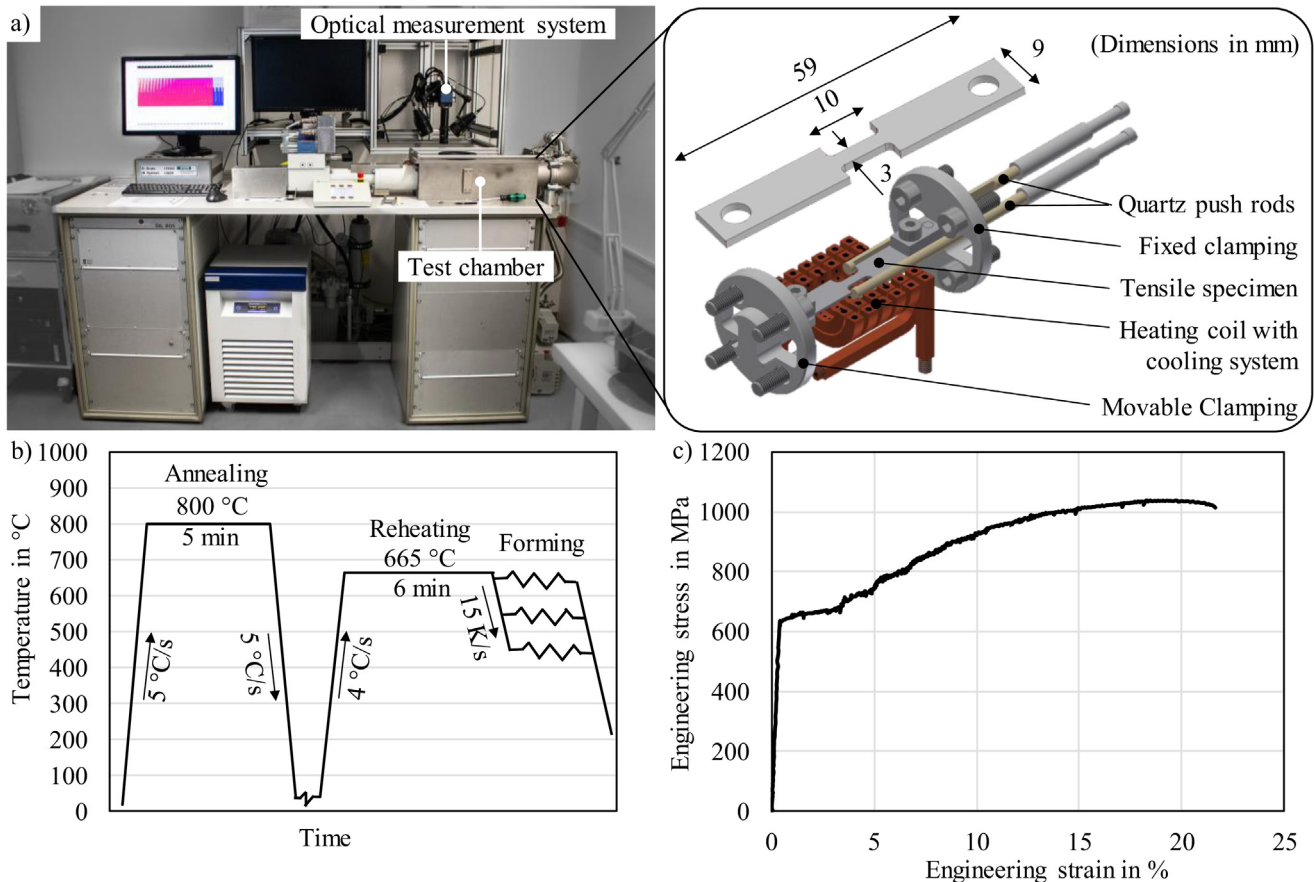


Fig. 1. (a) Dilatometer apparatus with the schematic test setup and specimen geometry [29] (b) applied heat treatment route, and (c) the engineering stress-strain curve of the medium Mn steel after heat treatment.

suitability of the experimental setup and the specimen geometry for determining flow curves was examined [30]. It was determined that a very good correlation with standardised tensile tests according to DIN EN ISO 6892-2 specification is achieved.

The tensile specimens were extracted from the rolling direction using water jet cutting, clamped between the fixed and movable holder and subsequently heated inductively with a heating coil. A type K thermocouple, which was welded onto the specimen surface, was used to measure and control the temperature during the test. The heat treatments involved annealing, cooling, reheating, forming and quenching to replicate the complete industrial process route. Annealing is carried out to simulate the final process step at the steel producer, while reheating, forming and quenching simulate the hot forming process at the parts manufacturer. In a preliminary investigation, optimal temperatures and durations for annealing and reheating were identified in order to find a promising combination of strength and ductility. Using the heat treatments depicted in Figure 1b, an ultimate tensile strength (UTS) of about 1039 MPa and a total elongation (TE) of 21.6% were attained after reheating. This corresponds to a product of UTS and TE of 22.4 GPa%, which is more than two times higher compared to conventional boron-added hot forming steels with UTS

levels of 1000 MPa and 1500 MPa (≤ 10 GPa% and ≤ 9 GPa%, respectively) [31]. The engineering stress-strain curve of the investigated medium Mn steel after heat treatment is shown in Figure 1c. For annealing, the tensile specimens were heated to a temperature of 800 °C at a rate of 5 °C/s and soaked at that temperature for 5 min. The soaking was followed by cooling to room temperature at a rate of 5 °C/s using helium. Then, the specimens were held at room temperature for 10 min, after which they were heated to a reheating temperature of 665 °C at a rate of 4 °C/s and soaked for 6 min. Subsequently, the specimens were cooled to the forming temperature with helium with a cooling rate of 15 °C/s to simulate the transfer to the forming die. Upon reaching the forming temperature, the specimens were isothermally tested at a constant strain rate until material failure occurred. Three forming temperatures of 450, 550, and 650 °C and three strain rates of 0.01, 0.1, and 1 s⁻¹ were analysed. Each test was conducted three times. In a previous work [28], the elongation Δl of the specimen was measured with two quartz push rods from the dilatometer. In contrast, in the present study, the elongation was measured with the in-situ optical measurement system Aramis from GOM GmbH. Therefore, a stochastic pattern was applied to the surface of each specimen before the test. Digital image correlation (DIC) was used to calculate the local strains ε of the specimen.

With this approach, higher true strains could be evaluated compared to the push rods because a local evaluation area could be defined within the parallel length of the specimens, neglecting the influence of the radii of the tapered area. The true stress σ and true plastic strain ε were calculated with equations (1) and (2).

$$\sigma = \frac{F}{A_i} = \frac{Fl}{A_0 l_0} = \frac{F}{A_0} \left(1 + \frac{\Delta l}{l_0}\right) \quad (1)$$

$$\varepsilon = \ln\left(\frac{l}{l_0}\right) = \ln\left(1 + \frac{\Delta l}{l_0}\right). \quad (2)$$

F represents the forming force, A_0 and l_0 the initial cross-sectional area and length and A_i and l the instantaneous cross-sectional area and length of the gauge section. Industrial forming processes usually lead to higher strains compared to the tensile tests. To enable an extrapolation of the experimental flow curve, it must be modelled with a suitable hardening law. Various phenomenological laws are available in the literature to describe the plastic deformation at elevated temperatures and strain rates. Johnson and Cook (JC) introduced a widely-used constitutive model for the calculation of the true stress σ taking strain hardening, strain rate $\dot{\varepsilon}$ and temperature T (in K) into account [32].

$$\sigma = (A + B\varepsilon^n)(1 + C \ln \frac{\dot{\varepsilon}}{\dot{\varepsilon}_0}) \left(1 - \left(\frac{T - T_r}{T_m - T_r}\right)^m\right). \quad (3)$$

A , B , C , m , n and $\dot{\varepsilon}_0$ are material specific constants that need to be fitted to the experimental flow curves. A is the initial yield stress at quasi-static strain rate and room temperature, B is the work hardening coefficient and n the hardening index, C is the strain rate sensitivity coefficient and $\dot{\varepsilon}_0$ the reference strain rate. T_r is a reference temperature, T_m is the melting temperature and m the temperature softening index. Ji et al. applied the JC law to model the hot deformation behaviour of 22MnB5 grade [33]. Since the model showed large fitting errors for the flow stresses at high temperatures, it was modified by a temperature-sensitivity coefficient D .

$$\sigma = (A + B\varepsilon^n)(1 + C \ln \frac{\dot{\varepsilon}}{\dot{\varepsilon}_0}) \left(1 - D \left(\frac{T - T_r}{T_m - T_r}\right)^m\right). \quad (4)$$

Hensel and Spittel (HS) also proposed a hardening law that considers strain hardening and softening, strain rate as well as temperature [34].

$$\sigma = A e^{m_1 T} \varepsilon^{m_2} \dot{\varepsilon}^{m_3} e^{\frac{m_4}{\varepsilon}} (1 + \varepsilon)^{m_5} T e^{m_6 \varepsilon} \dot{\varepsilon}^{m_7} T^{m_8}. \quad (5)$$

A and m_{1-8} are constants that depend on the material and are calibrated to the experimental flow curves [35]. The sensitivity of the material to the temperature is described by m_1 and m_8 . Coefficient m_5 defines the coupling between temperature and strain and m_7 defines the coupling between temperature and the strain rate. The coefficients m_2 , m_4 , and m_6 determine how sensitive the material is to strain changes and m_3 describes the strain rate sensitivity

of the material. The HS law was used by Tang et al. to model the plastic deformation of 22MnB5 grade in the hot forming simulation of a Nakajima test [36]. The applicability of the HS law for 22MnB5 steel was demonstrated by a strong agreement between the fitted flow model and the experimental data. Lechler et al. also characterised the material properties of 22MnB5 grade for the simulation of hot forming [21]. The plastic deformation was modelled using the constitutive law from Norton-Hoff (NH), which represents a modification and simplification the HS law [37].

$$\sigma = A e T^\beta \varepsilon^n \dot{\varepsilon}^m. \quad (6)$$

Merklein and Lechler extended the NH law to account for the initial yield stress, work hardening, and strain rate sensitivity [38].

$$\sigma = A e T^\beta (b + \varepsilon)^{n_0} e^{-c_n(T-T_0)} \varepsilon^{m_0} e^{c_m(T-T_0)}. \quad (7)$$

The parameters A , β , b , n_0 , c_n , m_0 , c_m denote constants that are specific to the material. T_0 represents the lower temperature limit of the hot forming process.

The hardening laws given above have been demonstrated to apply to 22MnB5 grade, but not for medium Mn steels. To assess their suitability for the hot forming simulation with a medium Mn steel, the model coefficients are calibrated to the experimental determined flow curves of the medium Mn steel investigated in this study. The model coefficients are adjusted to the experimental flow curves by minimizing the sum of the least squares between the experimental flow stress and the flow stress predicted by the hardening laws. After calibration, the flow curves are extrapolated and implemented into a material card in Abaqus. In order to verify the modelling accuracy, a thermo-mechanical FE model of the tensile test is calculated and the resulting force-displacement curves are compared to the experimental data. Figure 2 depicts the FE model with the corresponding boundary conditions. Hexahedral elements are used to mesh the tensile specimen with a global element edge length of 0.1 mm and a refined length of 0.075 mm in the gauge area of the specimen. To minimise computation time, only a quarter of the geometry was modelled and symmetry boundary conditions were applied. Similar to the experiment, one side of the specimen was constrained, while a specified displacement was applied to the opposite side until the maximum length change recorded in the experiment occurred. An implicit solver with automatic incrementation was used.

3 Results and discussion

The experimental flow curves were assessed by calculating the true stress and true plastic strain based on equations (1) and (2). The resulting curves for the investigated forming temperatures and strain rates are given in Figure 3. True stress decreases strongly with higher forming temperatures and increases moderately with higher strain rates. The highest true plastic strains are reached at the lowest forming temperature of 450 °C. It is evident that with

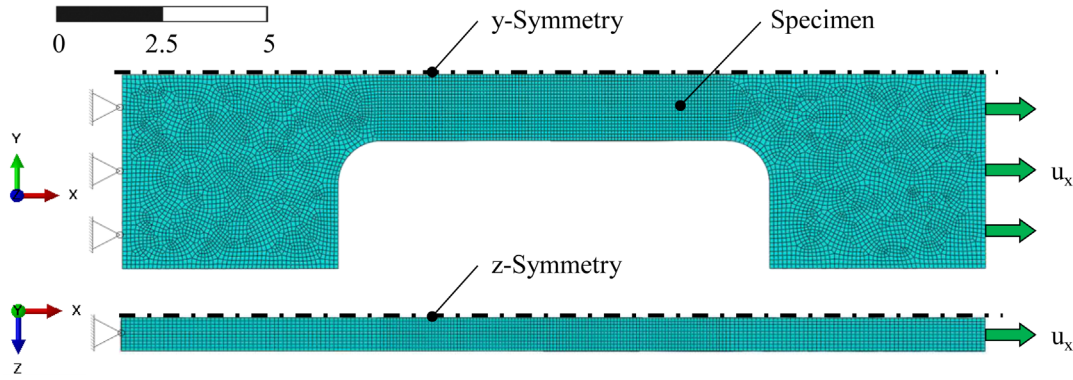


Fig. 2. FE model of the tensile test.

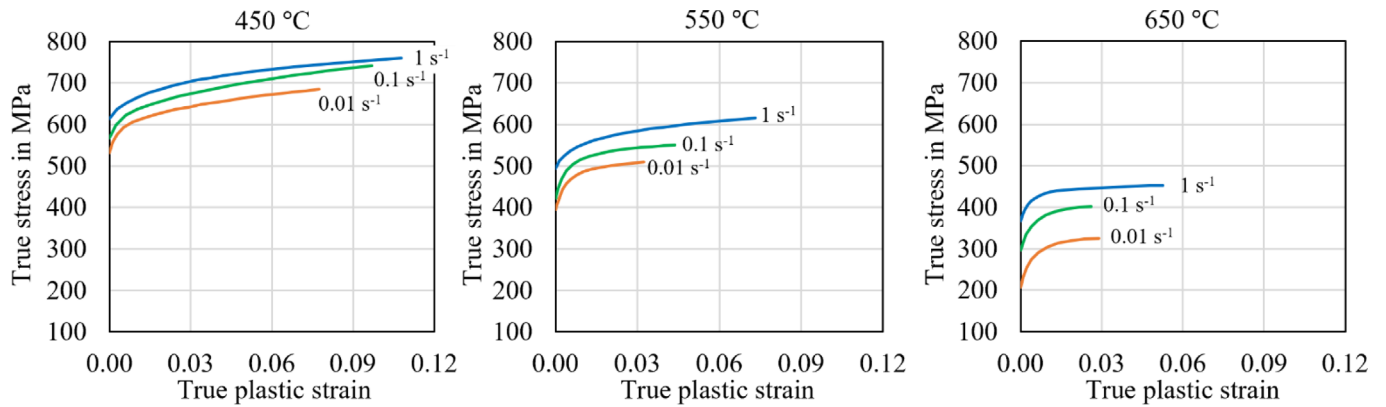


Fig. 3. Flow curves of the medium Mn steel for the investigated forming temperatures and strain rates.

Table 1. Model coefficients for the medium Mn steel determined from various hardening laws.

Mod. JC	A (MPa)	B (MPa)	C	D	m	n			
	405.0233	802.6690	0.0347	2.3948	1.6212	0.1241			
HS	A (MPa)	m_1	m_2	m_3	m_4	m_5	m_6	m_7	m_8
	3365.35	-0.00218	0.00031	-0.16565	-0.00045	0.00139	-0.02345	0.00025	0.00029
Mod. NH	A (MPa)	β (K)	b	n_0	c_n	m_0	c_m		
	346.86	636.67	2.6785×10^{-5}	0.02381	-0.00375	0.00316	0.00789		

higher forming temperatures, lower true plastic strains are obtained because of an earlier necking during the tensile tests. Once the material reaches the UTS, a further evaluation of the flow curve is not possible because a multiaxial stress state is present due to the aforementioned necking of the specimen.

The experimental flow curves were subsequently used to fit the coefficients of the modified JC, HS and modified NH hardening laws to enable an extrapolation to higher true strains. Consequently, the model coefficients were adjusted by minimising the sum of the least squares between the experimental flow stress and the prediction by the hardening laws. For the modified JC law, a strain rate parameter $\dot{\epsilon}_0$ of 0.001 and a melting temperature T_m of 1470 °C was assumed [33]. Table 1 provides a summary of the determined model coefficients.

Figures 4a, 4b and 4c show a comparison of the predicted flow curves with the experimental results to evaluate the prediction accuracies of the hardening laws for different hot forming temperatures at the strain rates of 0.01, 0.1, and 1 s⁻¹, respectively. It can be seen that the HS law shows a slight underestimation of the true stress for the forming temperature of 550 °C at the strain rates of 0.01 s⁻¹ and 0.1 s⁻¹. It also exhibits higher deviations at the prediction of the initial yield stress. This is due to the fact that the stress converges against zero for small strains because of its mathematical formulation. The modified JC and NH laws demonstrate a better prediction of the initial yield stress and show an overall good agreement to the experimental data. However, both models show deviations from the experimental results for the highest strain rate of 1 s⁻¹ and the highest forming temperature of 650 °C. For a

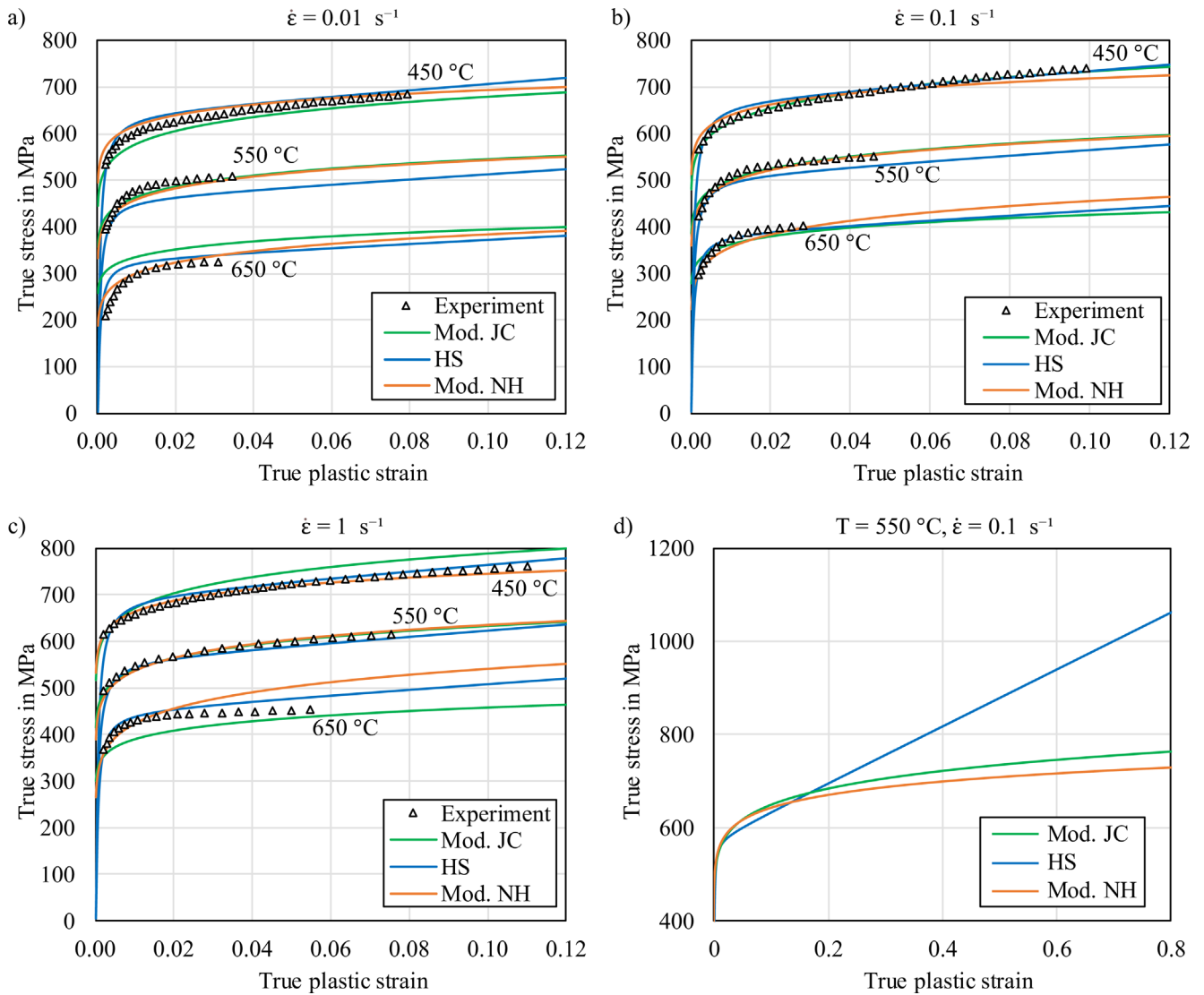


Fig. 4. (a) Comparison of different hardening laws for the modelling of the experimental flow curves at different hot forming temperatures for the strain rates of (a) 0.01 s^{-1} (b) 0.1 s^{-1} , and (c) 1 s^{-1} ; (d) representative extrapolated flow curves extending to higher true strains for the hot forming temperature of $550 \text{ }^\circ\text{C}$ and the strain rate 0.1 s^{-1} .

better quantification of the prediction accuracy of the hardening laws, the root mean square error (RMSE) and the coefficient of correlation R^2 between the predicted and experimental flow stresses were calculated for all conditions. It was found that the modified NH law provides the best prediction accuracy with an RMSE of 14.4 MPa and R^2 of 0.989. The HS law reached an RMSE of 18.7 MPa and R^2 of 0.964 and the modified JC an RMSE of 24.0 MPa and R^2 of 0.986.

Figure 4d shows the predicted work hardening behaviour extending to much higher strains. Since each model showed the same tendency for all temperatures and strain rates, as a representative case the extrapolation is only shown for the hot forming temperature of $550 \text{ }^\circ\text{C}$ and the strain rate 0.1 s^{-1} . It can be observed that the modified JC and modified NH laws are similar and show a lower work hardening effect compared to HS at elevated strains.

For a validation, the flow curves were implemented in Abaqus to simulate an additional tensile test, which was not used for the model calibration. This test was carried out at a forming temperature of $500 \text{ }^\circ\text{C}$ and a strain rate of 0.05 s^{-1} . Figure 5 shows a comparison of the numerical force over displacement with the experimental results. The HS law shows a slight underestimation of the forming force at the onset of plastic deformation. At higher displacements, the force is increasingly overestimated resulting in a significant deviation at fracture. This can be attributed to the higher work hardening behaviour of the model shown in Figure 4d. In contrast, the modified JC and NH laws show a better approximation of the experimental results. After a good predictive capability for the initiation of plastic deformation, both models show a slight overestimation after the onset of necking. Overall, the modified NH law shows a marginally better agreement to the experimental data especially at the displacement at fracture, which led to

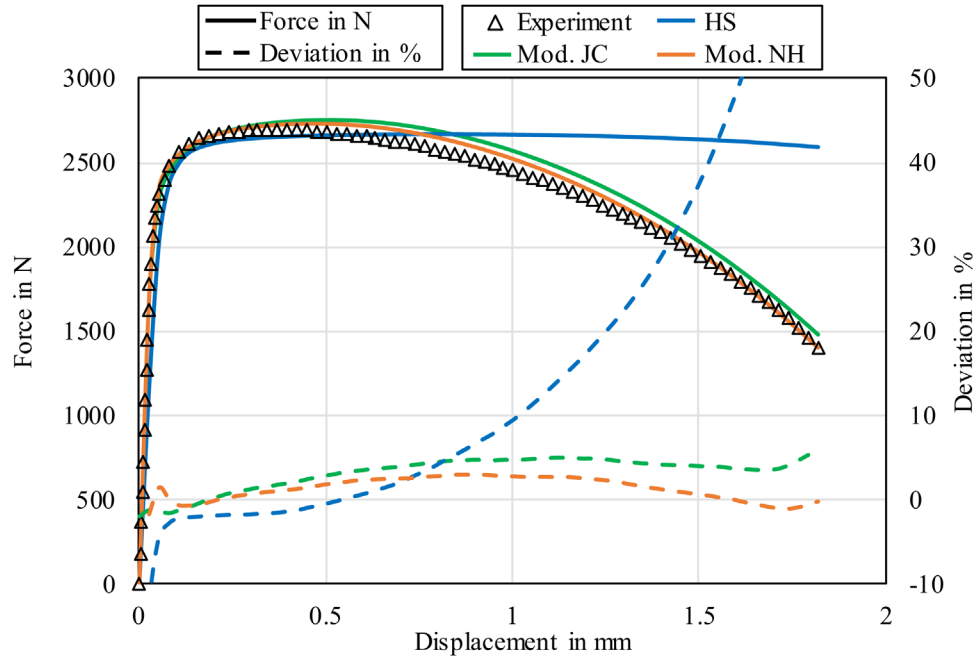


Fig. 5. Comparison of numerical and experimental force-displacement curves for a tensile test at 500 °C with a strain rate of 0.05 s⁻¹.

the lowest mean absolute percentage error (MAPE) of 1.3%. The modified JC law provides a MAPE of 3.4% and the HS law shows a significant MAPE of 17.6% due to the increasing deviation at higher displacements.

As evident from the A_{c1} and A_{c3} of the medium Mn steel given in Section 2, the relatively low hot forming temperatures used in the present work (450–650 °C) fall all in the intercritical temperature range of the steel and the preceding heat treatment before reheating of the material for hot forming was annealing of the cold rolled condition at 800 °C for 5 min (Fig. 1b). Therefore, the recovery and recrystallisation phenomena of the alloy took place during the annealing preceding hot forming and the starting material for hot forming was a fully annealed condition. Therefore, during hot deformation at the low forming temperatures, apparently not much driving force was available for recovery and recrystallisation to take place. This is evident from the flow curves in Figure 4 where the stress monotonically increases with strain without any sign of softening. Thus, the modelling approaches used by Li et al. [23] and Yan et al. [24] that consider recovery and recrystallisation, using much higher forming temperatures than in the current study, are not fully applicable here. However, as shown by Li et al. [25], the presence of ferrite in austenite in case of intercritical hot forming in the current study led to the appearance of the peak stress at relatively low strains (Fig. 4). Therefore, future research would focus on an extension of the experimental flow curves using appropriate experimental tests which enable higher strains to be reached, such as the plane strain compression test. This can improve the model calibration and enhance the prediction accuracy of the hardening laws at higher strains. Moreover, to gain a more profound insight into the influences of phases and their distribution in-situ measurements of deformation and microstructure evolution in an electron microscope would be useful.

4 Conclusion

The investigated Mn steel offers a high potential for energy savings since it can be hot formed at lower temperatures compared to conventional boron steels like the 22MnB5 grade. In addition, it can exhibit a promising combination of ductility and strength, which makes it a promising material for lightweight automotive components. The temperature has the greatest effect on the plastic deformation behaviour during forming. The true stress decreases strongly with higher forming temperatures and increases moderately with higher strain rates. To accurately model the flow behaviour in the hot forming-relevant process range, the applied hardening laws must consider the influence of strain hardening, strain rate and temperature. The hardening laws which are well-established and widely used for 22MnB5 grade, were successfully applied to the examined medium Mn steel.

The hardening laws demonstrated good predictive accuracy of the experimental true stress during model calibration. However, large differences were observed in the simulation of a validation test that was not used for modelling. The HS law showed deviations in the initial yield stress due to its mathematical formulation and overestimated the forming force at higher displacement due to a strong work hardening behaviour. Modified JC law showed the highest RMSE in the model calibration, but it provided a sufficient prediction of the forming force in the simulation of the validation test. The modified NH law provided the lowest RMSE of 14.4 MPa during fitting and achieved the best prediction of the forming force in the simulation with a MAPE of 1.3%. Therefore, the modified NH law is found to be most promising for the simulation of industrial hot forming processes with the considered medium Mn steel.

Funding

Funded by the Deutsche Forschungsgemeinschaft (DFG, German Research Foundation) - 505217238

Conflicts of interest

The authors have nothing to disclose.

Data availability statement

All the final data generated and analyzed during this study are included in this article.

Author contribution statement

Conceptualization, P.A., R.R. and H.W.; Methodology, P.A. and R.R.; Software, P.A.; Formal Analysis, P.A.; Investigation, P.A.; Resources, P.A., R.R. and B.-A.B.; Data Curation, P.A.; Writing – Original Draft Preparation, P.A.; Writing – Review & Editing, R.R., H.W. and J.U.; Visualization, P.A.; Supervision, H.W. and B.-A.B.; Project Administration, J.U. and B.-A.B.; Funding Acquisition, B.-A.B.

References

1. C.A. Romero, P. Correa, E.A. Ariza Echeverri, D. Vergara, Strategies for reducing automobile fuel consumption, *Appl. Sci.* **14** (2024) 910
2. R. Rana, S.B. Singh, *Automotive steels: design, metallurgy, processing and applications*, Elsevier/Woodhead Publishing, 2017
3. B.-A. Behrens, A. Bouguecha, C.M. Gaebel, J. Moritz, J. Schrödter, Hot stamping of load adjusted structural parts, *Procedia Eng.* **81** (2014) 1756–1761
4. K. Mori, P.F. Bariani, B.-A. Behrens, A. Brosius, S. Bruschi, T. Maeno, M. Merklein, J. Yanagimoto, Hot stamping of ultra-high strength steel parts, *CIRP Annals* **66** (2017) 755–777
5. M. Merklein, M. Wieland, M. Lechner, S. Bruschi, A. Ghiotti, Hot stamping of boron steel sheets with tailored properties: a review, *J. Mater. Process. Technol.* **228** (2016) 11–24
6. H. Wang, F. Yan, Z. Chang, A hot-stamped medium-mn steel with superior strength–ductility–bendability combination and thin oxidation layer, *Steel Res. Int.* **95** (2024). <https://doi.org/10.1002/srin.202300553>
7. R. Rana, T. Kop, P. Beentjes, E. van der Aa, Low temperature hot press forming of a zinc coated third generation advanced high strength steel, *MSF* **1105** (2023) 225–230
8. E. van der Aa, R. Rana, Optimization of hot forming temperature to minimize liquid metal embrittlement induced cracking in resistance spot welded zinc-coated medium manganese steel, *Steel Res. Int.* **94** (2023). <https://doi.org/10.1002/srin.202300045>
9. R. Rana, C.H. Carson, J.G. Speer, Hot forming response of medium Mn transformation induced plasticity steels, in: *Proceedings of 5th International Conference on Hot Sheet Metal Forming of High-Performance Steel (CHS2 2015)*, 31 May - 3 June 2015, AIST, Toronto, Ontario, Canada, 2015, pp. 391–399
10. R. Rana, T. Kop, Innovative hot forming of a Zn-coated medium Mn steel, in: *Proceedings of the 4th International Conference on Medium and High Manganese Steels (HMnS2019)*, April 1-3 2019, Aachen, Germany, 2019, pp. 299–302
11. W. Ding, N. Zhang, G. Zhang, Y. Li, M. Zhang, Microstructure and mechanical properties of medium manganese steel with different aluminum addition after very short time intercritical annealing, *J. Mater. Eng. Perform.* **33** (2024) 2015–2026
12. S. Chang, Z. Zhu, X. Huang, J. Zhang, G. Kang, Effect of martensitic transformation on ratchetting in medium-manganese steel: Experiment and homogenized constitutive model, *Int. J. Fatigue* **181** (2024) 108118
13. J. Speer, R. Rana, D. Matlock, A. Glover, G. Thomas, E. de Moor, Processing variants in medium-Mn steels, *Metals* **9** (2019) 771
14. R. Rana, P.J. Gibbs, E. de Moor, J.G. Speer, D.K. Matlock, A composite modeling analysis of the deformation behavior of medium manganese steels, *Steel Res. Int.* **86** (2015) 1139–1150
15. R. Rana, Special issue on ‘Medium manganese steels’, *Mater. Sci. Technol.* **35** (2019) 2039–2044
16. C. Wang, X. Li, S. Han, L. Zhang, Y. Chang, W. Cao, H. Dong, Warm stamping technology of the medium manganese steel, *Steel Res. Int.* **89** (2018). <https://doi.org/10.1002/srin.201700360>
17. Y. Chang, C.Y. Wang, K.M. Zhao, H. Dong, J.W. Yan, An introduction to medium-Mn steel: metallurgy, mechanical properties and warm stamping process, *Mater. Des.* **94** (2016) 424–432
18. S. Ge, Q. Wang, J. Wang, The impact wear-resistance enhancement mechanism of medium manganese steel and its applications in mining machines, *Wear* **376-377** (2017) 1097–1104
19. O.G. Bilir, T. Aycan Baser, A. Karşı, A. Bayram, E. Erisir, Modeling and simulation of hot stamping process for medium manganese steel alloy, *Int. J. Mater. Form.* **15** (2022). <https://doi.org/10.1007/s12289-022-01707-2>
20. G. Zheng, X. Li, Y. Chang, C. Wang, H. Dong, A comparative study on formability of the third-generation automotive medium-Mn steel and 22MnB5 steel, *J. Mater. Eng. Perform.* **27** (2018) 530–540
21. J. Lechler, M. Merklein, M. Geiger, Determination of thermal and mechanical material properties of ultra-high strength steels for hot stamping, *Steel Res. Int.* **79** (2008) 98–104
22. C. Tong, Q. Rong, V.A. Yardley, Z. Shi, X. Li, B. Zhang, D. Xu, J. Lin, Investigation of deformation behaviour with yield point phenomenon in cold-rolled medium-Mn steel under hot stamping conditions, *J. Mater. Process. Technol.* **306** (2022) 117623
23. B. Yin, Y. Han, W. Wang, H. Li, Y. Liu, X. Ran, Flow characteristics of a medium–high carbon Mn-Si-Cr alloyed steel at high temperatures, *J. Mater. Eng. Perform.* **28** (2019) 5104–5115
24. N. Yan, H.-S. Di, H.-Q. Huang, R.D.K. Misra, Y.-G. Deng, Hot deformation behavior and processing maps of a medium manganese TRIP steel, *Acta Metall. Sin. (Engl. Lett.)* **32** (2019) 1021–1031

25. Z. Li, R. Zhang, C. Luo, S. Du, H. Qi, W. Yang, The effect of the heating process on the warm deformation behavior and microstructure of medium Mn steel, *Steel Res. Int.* **96** (2025) 114–122
26. Y. Xu, P. Birnbaum, S. Pilz, X. Zhuang, Z. Zhao, V. Kräusel, Investigation of constitutive relationship and dynamic recrystallization behavior of 22MnB5 during hot deformation, *Results Phys.* **14** (2019) 102426
27. Q. Zhou, P. Guo, F. Qin, Stress response behavior, microstructure evolution and constitutive modeling of 22MnB5 boron steel under isothermal tensile load, *Metals* **12** (2022) 930
28. P. Althaus, R. Rana, H. Wester, J. Uhe, B.-A. Behrens, Characterisation and modelling of the flow behaviour of a medium manganese steel for hot forming, *MATEC Web Conf.* **408** (2025) 1058
29. B.-A. Behrens, D. Rosenbusch, H. Wester, E. Stockburger, Material characterization and modeling for finite element simulation of press hardening with AISI 420C, *J. Mater. Eng. Perform.* **31** (2022) 825–832
30. B.-A. Behrens, A. Bouguecha, M. Kammler, J. Schrödter, T. Hadifi, T. Götze, Assessment of a modified tensile specimen geometry for the characterization of 22MnB5 with a quenching and deformation dilatometer, in: *Proceedings of IDDRG 2012*, 25 - 29 November 2012, Bombay, India, 2012
31. P. Samadian, A. Abedini, C. Butcher, M.J. Worswick, Microstructure-based modelling of flow and fracture behavior of tailored microstructures of Ductibor[®] 1000-AS steel, *Metals* **12** (2022) 1770
32. G.R. Johnson, W.H. Cook, A constitutive model and data for metals subjected to large strains, high strain rates and high temperatures, in: *Proceedings of the 7th International Symposium on Ballistics*, The Hague, The Netherlands (April 1983), 1983, pp. 541–547
33. H. Ji, Y. Wen, G. Cui, W. Pei, W. Xiao, Hot-deformation behavior and processing map of 22MnB5 high-strength steel, *Mater. Tehnol.* **57** (2023). <https://doi.org/10.17222/mit.2023.874>
34. A. Hensel, T. Spittel, *Kraft- und Arbeitsbedarf bildsamer Formgebungsverfahren*, VEB Deutscher Verlag für Grundstoffindustrie, 1978
35. L. Niu, Q. Zhang, B. Wang, B. Han, H. Li, T. Mei, A modified Hansel-Spittel constitutive equation of Ti-6Al-4V during cogging process, *J. Alloys Compd.* **894** (2022) 162387
36. B.T. Tang, S. Bruschi, A. Ghiotti, P.F. Bariani, An improved damage evolution model to predict fracture of steel sheet at elevated temperature, *J. Mater. Process. Technol.* **228** (2016) 76–87
37. N.J. Hoff, Approximate analysis of structures in the presence of moderately large creep deformations, *Quart. Appl. Math.* **12** (1954) 49–55
38. M. Merklein, J. Lechler, Determination of material and process characteristics for hot stamping processes of quenchenable ultra high strength steels with respect to a FE-based process design, *SAE Int. J. Mater. Manf.* **1** (2009) 411–426

Cite this article as: Philipp Althaus, Radhakanta Rana, Hendrik Wester, Johanna Uhe, Bernd-Arno Behrens, Prediction of the hot flow behaviour of a third generation advanced high-strength hot-formable steel, *Manufacturing Rev.* **13**, 7 (2026), <https://doi.org/10.1051/mfreview/2026002>